N O T I C E

THIS DOCUMENT HAS BEEN REPRODUCED FROM
MICROFICHE. ALTHOUGH IT IS RECOGNIZED THAT
CERTAIN PORTIONS ARE ILLEGIBLE, IT IS BEING RELEASED
IN THE INTEREST OF MAKING AVAILABLE AS MUCH
INFORMATION AS POSSIBLE

Viking Lander Camera Geometry Calibration Report

Volume I: Test Methods and Data Reduction Techniques

Michael B. Wolf

April 15, 1981

Viking Lander Camera Geometry Calibration Report

Volume I: Test Methods and Data Reduction Techniques

Michael B. Wolf

April 15, 1981

PREFACE

The work in this two-volume report was conducted in the Image
Processing Laboratory by the Observational Systems Division of the
Jet Propulsion Laboratory.

Volume I describes the test methods and data reduction techniques
used to determine and remove instrument signature from Viking Lander
camera geometric data.

Volume II contains source listings of the computer programs used to
remove the instrument signature, computer printouts of test databases,
and Science Test Lander test results. Volume II is published separately
as a microfiche package, and is available from the Technical Documenta-
tion and Materiel Services Division, Jet Propulsion Laboratory, 4800 Oak
Grove Drive, Pasadena, California, 91109.

ACKNOWLEDGMENT

The efforts of many people were directed toward making this test
program meaningful and complete to the last detail. Among those who
contributed to the success of the tests were: Ed Green, Jack Donahue,
and Cliff Maxwell of Itek, Phil Avrin and Steve Carman of Martin Marietta
Aerospace (MMA), and David Atwood of Informatics.

ABSTRACT

This report describes the test methods and data reduction techniques used to determine and remove instrument signature from Viking Lander camera geometric data. Included are detailed descriptions of all tests, a listing of the final database ("calibration constants") used to remove instrument signature from Viking Lander flight images, and an exhaustive section on the theory of the geometric aberrations inherent in the Viking Lander camera. The database mentioned above, (included in Volume I), along with the computer programs listed in Volume II, will allow the reader to remove instrument signature from Viking Lander camera images.

CONTENTS

CONTENTS (Continued)

Tables

Figures

CONTENTS (Continued)

1. INTRODUCTION

The Viking Lander camera, built by Itek Corporation, underwent extensive geometric tests at Itek, Martin Marietta (MMA) and Kennedy Space Center (KSC). Also, the azimuth and elevation servos underwent periodicity error tests at the vendor (Clifton Precision, Litton Systems, Inc.). With the exception of the tests designed by the Image Processing Laboratory, (IPL) and run at MMA and KSC, none of these tests were designed to calibrate the camera geometrically. Rather, they were intended to demonstrate the compliance or noncompliance of the camera with project-defined specifications. Since this document concerns itself only with the calibration[1] of the camera, the non-IPL tests (with the exception of the surveying test at MMA) will not be discussed. The reader is referred to the calibration reports written by Itek for each camera which were delivered to MMA with the cameras. These earlier reports contain detailed results of the Itek geometric testing. A general description of the camera geometry is included in Section 3.

2. EARLY WORK AT ITEK AND MMA

2.1 VLIS Image Quality Analysis Report

Itek produced an early study (October 1972) of the cameras' predicted performance called the "VLIS Image Quality Analysis Report." This document considered camera radiometry, geometry and also GRE performance (the GRE is a laser film recording device).

---

[1]In this report, we define "calibration" to mean the process of gathering and reducing the data necessary to infer object space pointing directions from image coordinates.

In section 3, the author points out that the Viking Lander camera is not an ideal facsimile camera, but an array of photodetectors (none of which is on-axis), a lens, a mirror whose rotation axis does not lie in the plane of the mirror's reflecting surface and one, or optionally two, windows. The implications of this difference are discussed in detail. Scalar equations expressing the ray offset resulting from the true versus nominal ray path are derived. Nearly all of these equations are derived in an approximation form, with the elevation and azimuth errors considered separately. Plots of the displacements versus elevation for each of the major aberrations are presented.

The major problem with this camera configuration is that it implicitly implies a moving coordinate system origin. Thus, the statement that the angular error is just the displacement divided by the range is not true. The real situation is more complex. Another minor problem is that is fails to consider effects that are hard or impossible to visualize. In other words, one must be able to visualize the entire optical system in 3-space and then visualize all the nonideal effects and write down equations which accurately describe them. The advantage of the raytrace method described in this report is that this is unnecessary: all of the aberrations fall out of the model without any visualization being necessary.

A major contribution of the VLIS report is that it alerted many people as to the magnitude of the nonideal nature of the Viking Lander camera.

2.2   The Martin Marietta Pointing Accuracy Test

Martin Marietta designed a "camera pointing accuracy" test to be
run on the Flight Landers at MMA in the high bay area during subsystem
verification testing. An edge target (an opaque right angle, backlit by
a diffuse source) was imaged and accurately surveyed with respect to the
camera coordinate system origin. Since the coordinates of both the target
and the camera coordinate system origin are known in the same coordinate
system, the apparent azimuth and elevation of the target, as seen by the
camera, can be calculated. This can then be compared to the azimuth and
elevation of the target derived from image coordinates. This will allow
the calculation of constant pointing errors in azimuth and elevation.
Since there was only one target, it had to be resurveyed for each new
position. This required the nearly continuous and simultaneous availa-
bility of the personnel to do the surveying, imaging and target setup.
It also practically limited the number of points that could be used.

The test was only run once, on the PTC Lander at MMA. The results
are related in the PTC test document published by MMA. This test was
replaced by one designed by IPL for the Flight Lander Tests. See Section
4.2 of this report for a complete description of the test.

3.   THE CAMERA RAYTRACE MODEL

3.1   The Ideal Facsimile Camera

An ideal facsimile camera would consist of an on-axis photodetector,
a lens, and a scanning mirror. Such a device is shown in Figure 1. If
the camera rotated as a whole for azimuth scan and both azimuth and
elevation scanning were performed by digital servos, then the resulting
digital image would have a simple linear relationship between the image

coordinates of a given pixel and the azimuth and elevation of its pointing direction in space. That is, lines of constant azimuth and elevation in the digital image would be straight lines, and parallel to the image coordinate axes.

3.2 The Actual Camera

A schematic diagram of the actual camera is shown in Figure 2. Note that none of the diodes are on the optical axis. The diodes are actually placed in a 2- by 6-array, on a board called the Photosensor Array or PSA (a schematic of the PSA is shown in Figure 3.). Note that one, or optionally two, windows are in the optical path after the mirror. Originally there was only to be one window. The windows cause the ray to be offset at elevations other than 0°. This will lead to pointing angle errors at finite object distances on the order of the amount of the ray offset divided by the object distance. For this reason, Itek engineers decided to set the mirror rotation axis behind the mirror by 1/8 in. This has the effect of introducing an opposite and approximately equal offset in the ray for elevations below 0° (the most frequently used elevation regime). The idea was that this would nearly eliminate the variation of pointing angle errors with elevation in this regime. This turns out to be exactly the case. See Figure 4 for plots of the ray offsets for BB-2, BB-4, GREEN and RED as predicted by Itek. See Figure 5 for the actual range dependent elevation pointing errors derived from the raytrace model for lander 1, camera 1 (FC-1B), for the BB-2, BB-4, GREEN and RED diodes at 1.0 meters range. The great similarity of the curves is quite apparent. One is tempted to say that the angular errors presented in Figure 5 are just the positional offsets presented in Figure 4 divided by 1 meter. Actually, this in not the case. The displacements Itek

plotted in Figure 4 are the displacements of the ray from an on-axis ray to the ray from the actual diode. The displacements that are really relevant to the problem are the displacements of the ray itself from the coordinate system origin.

3.3   The Major Elevation Pointing Errors

3.3.1 Elevation Servo Nonlinearity

The elevation servos were calibrated for periodic error at the vendors. Maximum error was $\pm$ several arc minutes. IPL software for geometric decalibration could handle such data, but the test data could not be used. The IPL could not determine the phase relationship between test angles and camera command angles.

3.3.2 Elevation Zero Point or "Bolt-Down" Error

All constant offset errors in elevation are lumped together and called "elevation bolt-down errors." Contributors include any tilt of the mirror in elevation due to loose clamps, machining errors, etc.; failure to connect the mirror cage to the servo shaft at an angle other than the nominal; and positional shift of the PSA in the elevation direction.

3.3.3 Offset Due to Diode Positioning

The offset error is equal to the angular distance that the diode is off the optical axis. This distance is as great as 2.4° for some d' es (BB-1, BB-2, BB-3, and BB-4). This would cause a considerable error were it not for the fact that the camera electronics senses which diode has been commanded and introduces a compensatory correction into the mirror angle. This, of course, helps the situation immensely, but still leaves us with a problem. The true ray path from the object to the camera will not be parallel to the line from the object to the camera coordinate

5

system origin for finite object distances. This is because the ray from the object to the diode does not pass through the camera coordinate system origin. If the elevation of the object _relative to the camera coordinate system origin_ is inferred from image coordinates, we will be in error by an angle equal to the ray offset from the origin divided by the object distance. The error is approximately 0.1° for a broadband diode at 1.0 meters, but this effect is compounded by other effects, discussed below.

3.3.4 Offset Due to Window

At elevations other than 0°, the ray will be offset as it passes through the window. This offset may add or subtract to that of Paragraph 3.3.3, depending on whether we are imaging above or below 0° and on which diode is commanded. The offset is doubled if the contamination cover is in place.

3.3.5 Angular Error and Offset Due to Refraction

Since the pressure inside the camera is 530 torr of argon during flight and the pressure outside is 1 torr of carbon dioxide, the ray is refracted (bent) on its way through the window. The contamination cover is not sealed; hence, the pressure is the same on both sides, and no net refraction occurs as the ray passes through the contamination cover. The net refraction through the window causes an elevation-dependent elevation error (not range dependent). However, the refraction also causes a change in the offset, or the amount by which the ray misses the coordinate system origin. This combines with the offsets in Paragraphs 3.3.3 and 3.3.4 and, thus, contributes to the range dependent elevation error. Thus,

we see that refraction causes two elevation errors: one directly due to the refraction, which is not range dependent, and one due to the ray offset induced by the refraction, which is range dependent.

3.3.6 Ray Offset Due to Mirror Offset

As mentioned previously, the axis of rotation for the mirror does not lie in the plane of the mirror's reflecting surface, but, rather, is offset by 0.125 in. This causes the rays to be offset down from where they would have been if this had not been done. See Figure 6 for a diagram of this effect.

This effect is a minimum at a 45° mirror angle (to the horizontal) and increases away from the angle. The sign of the effect is such that the ray is always shifted down. The ray offset mentioned in Paragraph 3.3.4 due to the window thickness causes the ray to be offset up at elevations less than 0° and to be offset down at elevations greater than 0°. Hence, the "window thickness" and "mirror offset" effects tend to compensate (have opposite signs) below 0°, but tend to reinforce (have the same signs) above 0°. The plots in Figures 4 and 5 indeed show such a compensatory effect between -60° and 0°. The error quickly gets quite large above 0°; however, just as we predicted, as this is the regime where the "mirror offset" and "window thickness" effects add instead of cancel.

Unfortunately, after all this was figured out and built into the camera by Itek engineers, it was decided to add another window of the same thickness. The additional window could be opened by ground command, should the window's outer surface become covered with dust. With two windows, the error balancing scheme just described doesn't work. The 0.125-in. offset of the mirror calculated by Itek engineers balances the ray offset of

7

one window of 0.1000-in. thickness, not two windows of 0.1000-in. thickness. Figure 7 shows two plots. One is a BB-1 plot with the "window open" (one window). The other plot is the same, except the outer window is closed (two windows). This is the same as if we had only one window and had not offset the mirror. In other words, with the outer window closed, we are back where we started.

It must be remembered, however, that all of these offset effects (with the exception of the pure refraction part of Paragraph 3.3.5) are inversely proportional to object distance, and are all insignificant beyond 10 meters object distance (less than 0.3 high resolution pixels). On the other hand, the difference in elevation pointing direction between a BB-2 and BB-3 diode is approximately 5 to 6 high resolution pixels (0.2 → 0.4°) at an object distance of 1 meter.

In any event, all these effects are properly handled by the raytrace program, XLGEOM, discussed later.

3.4   The Major Azimuth Pointing Errors

3.4.1 Azimuth Bolt-Down Error

Because of a relatively large (±2°) tolerance in the mounting of the azimuth servos in the camera, object azimuths derived from image coordinates could have been in error by the same amount. The largest error for a flight camera is 0.92° (lander 1, camera 1).

3.4.2 Coning Angle Effect

Due to the fact that the diodes are not on the optical axis, the elevation scan lines in space are curves, not straight lines. In fact, the rays lie on the surface of a cone (see Figure 8). This effect is

8

elevation dependent and has the functional form:

$$\Delta\theta = \pm \tan^{-1} \left(\frac{\tan 0.48^\circ}{\cos \phi}\right) - 0.48^\circ \qquad (1)$$

where $\Delta\theta$ is the image space azimuth correction and ϕ is the elevation.
The plus sign is taken for diodes BB-2, BLUE, GREEN, RED, SUN and BB-4,
and the minus sign is taken for diodes BB-1, IR-3, IR-2, SURV and BB-3.
The coning angle effect is one of the most serious aberrations in the
Viking Lander camera for two reasons. First, it is a large effect
(0.48° at -60° elevation), and second, it is not range dependent. Hence,
we cannot ignore it even for very distant objects.

3.4.3 Offset Due to Diode Positioning

This is the same type of effect as mentioned in Paragraph 3.3.3
for elevation. The sign of the effect will depend on which of the two
rows of six the chosen diode lies in. This offset causes approximately
0.02° of azimuth error at an object distance of 1.0 meters. The effect
is inversely proportional to range. Figure 9 shows a plot of this effect
from the raytrace model for BB-2 diode, lander 1, camera 1, 1.0 meters
range. Note the strong elevation dependence. This is because the coning
effect (Paragraph 3.4.2) increases the amount that the ray misses the
coordinate system origin, actually doubling it at -60°. Note that the
azimuth error is twice as large at -60° as it is at 0°.

3.4.4 Offset Due to Window

The ray is shifted or offset in azimuth as it passes through the
window. Note that the net effect is to decrease the total offset of the
ray from the coordinate system origin. Thus, the net range dependent

azimuth dependent error should decrease when the contamination cover is in the optical path. This is exactly what the raytrace model predicts. In Figure 9 the upper curve is for the contamination cover open, the lower curve is for it closed.

3.4.5 Angular Error and Offset Due to Refraction

These are the same types of errors as described in Paragraph 3.3.5, but much smaller in magnitude. This is because the angle of incidence (in azimuth) is always small (less than 1°). The angular error due to the refraction itself is less than 0.0003° and the angular error at 1.0 meters due to the change in offset is less than 10^{-5} degrees. These are both certainly negligible.

3.5 The Raytrace Approach

With a knowledge of the positions of all the optical elements in the camera, it is possible to determine the path in space followed by a ray of light from a particular object point to a particular diode. Actually, the raytrace is done in reverse: it begins at the diode and in the end it gives us a pointing direction in space to the object point for a particular mirror position. Figure 10 is a diagram showing the internal relationship between the PSA and mirror, and Figure 11 shows the lens nodal points. Table 1 shows the coordinates of the center of each diode aperture. The units are inches, and the coordinate system is an internal PSA coordinate system. The origin of the system is at the center of the BB-2 diode aperture. The Y-axis points down (in the figure) and is parallel to the camera rotation axis; the X-axis points away from the window and is parallel to the PSA long axis; the system is right-handed.

The lens is assumed completely characterized by the knowledge of the position of its two nodal points. These points are also given in Table 1.

10

Table 1. Photodiode Center Coordinates

Diodes	Coordinates		
	$\bar{X}$	Y	$\bar{Z}$
BB-2	0.0	0.0	0.0
BLU	-0.036	0.0	+0.0029
GRN	-0.72	0.0	+0.0029
RED	-0.108	0.0	+0.0029
SUN	-0.144	0.0	-0.0013
BB-4	-0.180	0.0	+0.0337
BB-1	0.0	+0.036	-0.0169
IR-3	-0.036	+0.036	+0.0029
IR-2	-0.072	+0.036	+0.0029
IR-1	-0.108	+0.036	+0.0029
BB-3	-0.180	+0.036	+0.0168
SURV	-0.144	+0.036	-0.0013

The raytrace process begins by calculating the vector $\vec{V}_1$ from the selected diode aperture to the lower nodal point (see Figure 12). The next part of the ray path, $\vec{V}_2$, connects the lower to the upper nodal point, $\vec{V}_3$, is the vector from the upper nodal point to the mirror, and is parallel to $\vec{V}_1$. Hence, in vector notation, $\vec{V}_3 = \vec{V}_1$. The direction of the ray after reflection off the mirror is denoted by $\vec{V}_4$. $\vec{V}_4$ can be calculated from $\vec{V}_3$ by applying the law of reflection. To do this, one must know the exact position and orientation of the mirror. The law of reflection can be expressed (in 3 dimensions) by the left set of equations in Figure 13.

11

If we set OLD = $\vec{V}_3$ and NEW = $\vec{V}_4$, then the left set of equations in
Figure 13 applies to the situation at hand. Having solved for $\vec{V}_4$,
we are now faced with the problem of tracing the ray through either
one or two windows. The right set of equations in Figure 13 expresses
the law of refraction (Snell's Law) in 3 dimensions. We must solve
these equations once for each index-to-index interface that the ray
passes through, i.e., we must solve the equations twice for one win-
dow, or four times for two windows. After the raytrace program has
done all this, we are left with $\vec{V}_8$, the direction of the ray as it
exits the last optical surface of the system. (Note that $\vec{V}_8$ is not
necessarily parallel to $\vec{V}_6$, since the index of refraction of the gas
inside the camera does not equal the index of refraction of the gas
outside in the Martian atmosphere.)

The next vector that we must solve for is the one that points
from the camera coordinate system origin to the object: $\vec{U}_3$. Figure 14
is a diagram of all the relevant vectors. Vector $\vec{U}_1$ is a vector that
points from the coordinate system origin to the point where the ray exits
the last optical surface in the system. Vector $\vec{U}_2$ is a vector pointing
from the terminal point of vector $\vec{U}_1$ to the object point, P. Vector $\vec{U}_3$
points from the coordinate system origin to the object point. Vectors $\vec{U}_1$,
$\vec{U}_2$, $\vec{U}_3$ and their magnitudes and unit vectors are related as follows:

$$\vec{U}_1 = A\vec{u}_1 \tag{2}$$

$$\vec{U}_2 = B\vec{u}_2 \tag{3}$$

$$\vec{U}_3 = C\vec{u}_3 \tag{4}$$

where $\vec{u}_1$, $\vec{u}_2$, $\vec{u}_3$ are <u>unit</u> vectors in the directions of $\vec{U}_1$, $\vec{U}_2$, $\vec{U}_3$ respectively
and A, B, C are the magnitudes of vectors $\vec{U}_1$, $\vec{U}_2$, $\vec{U}_3$ respectively.

The raytrace procedure has already given us vectors U_1 and u_2. By referring to Figure 14 we can see that:

$$\vec{U_3} = \vec{U_1} + \vec{U_2} \qquad (5)$$

substituting,

$$\vec{U_3} = \vec{U_1} + (B\vec{u_2}) \qquad (6)$$

Also,

$$\vec{U_3} \cdot \vec{U_3} = C^2 \qquad (7)$$

Therefore,

$$c^2 = \overline{[\vec{U_1} + (B\vec{u_2})]} \cdot \overline{[\vec{U_1} + (B\vec{u_2})]} \qquad (8)$$

Evaluating the dot products on the right of Equation (8) we get:

$$B^2 + 2B(\vec{U_1} \cdot \vec{u_2}) + (A^2 - C^2) = 0 \qquad (9)$$

All factors in Equation (9) are known except B. Equation (9) is a quadratic equation in the independent variable B, the magnitude of $\vec{U_2}$ (C is the range or distance from the coordinate system origin to the object point). An approximate value for C must be known to solve for $\vec{U_3}$. Since $\vec{U_3}$ is a very slowly varying function of C, C need only be known to +25% for ranges <10 m, to give fractional pixel accuracy for the direction of $\vec{U_3}$. If C is known to be >10 m, it can be safely set to infinity without substantially affecting the solution for $\vec{U_3}$. The solution for B is:

$$B = [(\vec{U_1} \cdot \vec{u_2})^2 - (A^2 - C^2)]^{1/2} - (\vec{U_1} \cdot \vec{u_2}) \qquad (10)$$

Plugging B into Equation (6) we now can solve for $\vec{U_3}$, the vector from the coordinate system origin to the object point.

For the perfect camera already discussed (see Figure 1) the relationship between image line coordinate (elevation direction) and elevation is:

$$\phi = \phi_0 + R(256.5 - L) \qquad (11)$$

where ϕ is the elevation, ϕ_0 is the center of frame elevation (a camera command), R is the pixel spacing, and L is the line coordinate. This value of ϕ defines a vector, $\vec{U_4}$. $\vec{U_4}$ is the direction that an ideal camera would point for a line coordinate $\underline{L}$. In the coordinate system that $\vec{U_1}$, $\vec{U_2}$, and $\vec{U_3}$ are expressed in $\vec{U_4}$ can be written:

$$U_4(1) = \cos\phi \qquad (12)$$

$$U_4(2) = 0 \qquad (13)$$

$$U_4(3) = \sin\phi \qquad (14)$$

Since we can calculate the real direction to a finite distance object, $\vec{U_3}$, we can calculate corrections to apply to the image coordinate-derived azimuths and elevations which assume a "perfect" camera. The corrections can be written:

$$\Delta\phi = \text{elevation correction} = \sin^{-1}[U_4(3)] - \sin^{-1}[U_3(3)] \qquad (15)$$

$$\Delta\theta = \text{azimuth correction} = \tan^{-1}\left[\frac{U_3(2)}{U_3(1)}\right] \qquad (16)$$

If for a real (i.e., not an ideal) camera, we can compute the approximate azimuth and elevation of an object point from its image space coordinates using the following formulas:

14

$$\theta = \text{azimuth} = \theta_0 + R(S - 1) \qquad (17)$$

$$\phi = \text{elevation} = \phi_0 + R(256.5 - L) \qquad (18)$$

Then the corrections calculated in Equations (15) and (16) are applied as follows:

$$\theta^* = \theta + \Delta\theta \qquad (19)$$

$$\phi^* = \phi + \Delta\phi \qquad (20)$$

Where θ^* and ϕ^* are now the "true" azimuth and elevation, i.e., the azimuth and elevation relative to the camera coordinate system origin.

The complete transformation from image coordinates (line and sample) to object space coordinates (θ^*, ϕ^*), relative to the camera coordinate system origin, and the reverse transformation are handled by the Fortran subroutine XLGEOM. This subroutine accepts as input data the lander identification, the camera position, the channel identification (diode), the commanded mode, the contamination cover position (outer window), the camera-to-object distance (range), the image coordinates of the object of interest, and the camera starting azimuth and elevation command. From this data, and from camera parameter data which it reads from the calibration file, XLGEOM does a raytrace and computes $\vec{V}_6$ (or $\vec{V}_8$, if the contamination cover is closed), the vector direction of the ray of light from the object point as it enters the first exterior optical surface of the camera system. This vector is one of the arguments, or returned values, the XLGEOM calculates from the input data. XLGEOM also calculates and returns the point where the ray enters the optical system, i.e., the place where the ray pierces the first optical surface. The X, Y, Z coordinates of this point and the vector $\vec{V}_6$ (or $\vec{V}_8$) are returned to the user of XLGEOM expressed on the lander aligned coordinate system (LACS).

15

(This system has been in common use throughout the mission and has been defined before in many documents.) XLGEOM also calculates and returns θ^* and ϕ^* using the procedure outlined above.

XLGEOM will also handle the reverse transformation. In this case, the input arguments are θ^* and ϕ^* and the returned values are the image coordinates.

The transformation from image to object space, and vice versa, supplied by subroutine XLGEOM, is useful in applications such as calculating distance (range) to object points, given their image coordinates in a stereo pair of images (the IPL program RANGER uses XLGEOM).

4.   THE TESTS

4.1   Grid Target Test at Itek

During the flight acceptance tests at Itek, JPL arranged for a grid target to be imaged by each flight camera. The grid target was computer generated (on the IPL 360/44) and was reproduced photographically. The grid was white lines on a black background, and two targets were generated: one for low resolution imaging (0.12°) and one for high resolution imaging (0.04°). The width of each line was designed to subtend 1-1/2 pixels at 2 meters. This test was designed to study the "pixel jitter" of the system only, not to characterize the geometrical properties of the camera. As a result of this test, flight camera FC-2B was found to have an excessive amount of pixel jitter and was removed from its lander and replaced with another camera. For a complete description of the test and the numerical results, refer to Section 2 of this report.

16

4.2   Grid Target Test at MMA/KSC

Once at Martin Marietta (MMA) and again at Kennedy Space Center (KSC), each flight lander imaged a grid target whose position relative to the lander had been accurately surveyed. Figure 15 is an image of the grid target taken by flight lander number 1 at MMA. The target was drawn on mylar film by a calcomp plotter at USGS, Flagstaff. The mylar film was then glued to a 4-by 8-foot piece of aluminum jig plate. The jig plate was supported in a vertical plane by a very sturdy mount, weighing several tons (filled with sand). The black lines were 5.5 mm wide and were spaced 11 cm apart. The target plane was situated approximately 2.5 meters forward of the line joining the camera centers. It was not possible to survey every intersection (because of the closeness of the target to the lander), so only certain selected intersections were surveyed. Also, because of the peculiar surveying techniques employed, X, Y and Z coordinates could not all be measured for a given intersection (e.g., only X and Y could be measured for one intersection and only Z for yet another, etc.).

Program XVLGRID1 had to take the raw survey coordinates of a few selected intersections (with incomplete sets of X, Y and Z coordinates as mentioned above) and generate a disk data set containing X, Y and Z coordinates of all intersections on the target. After the survey was complete, the cameras were commanded to image the target. Five images were made with the BB-2 diode, 5 images with the survey diode, and 1 image each with the other diodes, for a total of 19 images. This entire sequence was repeated for both cameras. The entire test was performed both at MMA and later at KSC. Since there were two flight landers, this resulted in 152 images, ranging in size from 512 by 600 to 512 by 1500. Analyzing this enormous amount of information took many man-months.

17

5.   CALIBRATION FILE GENERATION

5.1   Calibration File Format

Each calibration file is VICAR labelled and consists of N 400-byte records, each record representing a single lander (data for both cameras are contained in the single record). Table 2 outlines the contents of the records. Each word is four bytes long, either in floating point or integer format (as specified). Subscripts (1 or 2) denote camera identification.

5.2   Camera Parameter Adjustment

Certain of the items in the calibration file are incrementally derived adjustments to nominal camera parameters. These are LENCOR, PSACOR, PSAROT, and PSASFT. LENCOR is a small adjustment of the lens position along the optical axis, PSACOR is a small adjustment of the PSA position along the optical axis, PSAROT is a small rotation off-nominal of the PSA around the optical axis, and PSASFT is a small shift of the PSA in the azimuth direction. The fact that the diodes are not located in the same physical spot in the image plane causes the rays from each diode to travel in a slightly different direction for a fixed mirror position (see Section 3). The four broadband diodes, being located at the extreme corners of the PSA, show the greatest divergence in pointing direction. If we have properly modelled the camera (i.e., if we know the precise locations of the diode apertures and the precise locations of each of the optical elements), and if we know the range to the object point, then we can properly infer the azimuth and elevation of the object point relative to the camera coordinate system origin, regardless of which diode was used to provide the image. This process we call "decalibration." If however, we do not know the precise locations of the optical elements, but only nominal ones, we can use the convergence of the pointing directions

18

Table 2. Viking Lander Camera Geometric Calibration
         File Format

Word	Quantity	Format	Description
1	Lander identification	Integer	Must be a 1 or 2 specifying which lander.
2	File type	Integer	Must be 0, 1 or 2. 0 implies nominal corrections only, 1 implies bolt down only, 2 implies incrementally derived adjustment of camera parameters.
3	Date	Integer	YYDDD, e.g., 77365 implies December 31, 1977. This is the date of file creation.
4	Not used	-	-
5	Not used	-	-
6	$EPSILON_1$	Floating	One of 3 angles defining camera to spacecraft rotational transformation; units = radians.
7	$EPSILON_2$	Floating	Ditto.
8	$DELTA_1$	Floating	Ditto.
9	$DELTA_2$	Floating	Ditto.
10	$THETA_1$	Floating	Ditto.
11	$THETA_2$	Floating	Ditto.
12	$PSACOR_1$	Floating	The best incremental adjustment to PSA position in the vertical direction (determined by program VLOPTICS); units = inches.
13	$PSACOR_2$	Floating	Ditto, but for camera 2.
14	$LENCOR_1$	Floating	The best incremental adjustment to lens position in the vertical direction (determined by program VLOPTICS); units = inches.
15	$LENCOR_2$	Floating	Ditto, but for camera 2.

Table 2. Viking Lander Camera Geometric Calibration
File Format (Continuation 1)

Word	Quantity	Format	Description
16	$PSAROT_1$	Floating	The best incremental adjustment to the PSA rotation (determined by program VLOPTICS); units = degrees.
17	$PSAROT_2$	Floating	Ditto, but for camera 2.
18	$ELOFFHI_1$	Floating	Elevation offset correction, for high resolution mode; units = radians.
19	$ELOFFHI_2$	Floating	Ditto, but for camera 2.
20	$ELOFFLO_1$	Floating	Elevation offset correction for low resolution mode; units = radians.
21	$ELOFFLO_2$	Floating	Ditto, but for camera 2.
22	$PSASFT_1$	Floating	The best incremental adjustment to the PSA position in the left-right sense (determined by program VLOPTICS); units = inches.
23[a]	$PSASFT_2$	Floating	Ditto, but for camera 2.

[a]Words 24 to 100 are reserved for future expansion (unused).

for the four broadband diodes as a success criteria for the calculation of a "best position" of a given optical element. The way the process works is as follows. We start with four images of the same object, in this case, a given intersection on the surveyed grid target. The four images are taken by the BB-1, BB-2, BB-3 and BB-4 diodes. The precise image coordinates of the intersection in each of the four images is found using a standard automatic grid intersection finding algorithm. These four sets

20

of coordinates are input one at a time to the raytrace program XLGEOM (See section 3.5) to produce four sets of (azimuth, elevation) coordinates for the object point. These four sets should be the same (since they are imaging the same physical object); but, due to our imprecise knowledge of the positions of optical elements, our model is not exact, so the four sets of coordinates will not be identical. The standard deviation of the mean of these four sets of coordinates is a good "figure of merit" to indicate to us how good our model is. Indeed, we can arrive at the "best" position for a given optical element by repeatedly invoking the raytrace program XLGEOM, each time incrementally adjusting one of the parameters such as the lens position, until a minimum in the standard deviation vs. parameter value curve is found. I have made the assumption that the value of the parameter (whether it is lens position, PSA position, rotation or PSA shift) that gives the minimum standard deviation of the mean of the four sets of coordinates is the "best" value (Figure 16 shows a typical convergence for a typical parameter adjustment). The program that does this for all parameters is called VLOPTICS. VLOPTICS is an interactive program. A sample printout is shown in Figure 17.

Once we have found the actual positions for the optical elements for a given camera, we know its internal geometry. Now we are left with the problem of relating it in space to the lander coordinate system (its external geometry). For this we must depend on surveyed grid target intersections that have been photographed by the camera. By means of the survey, the precise locations (accurate to about 0.5 mm) of the intersections relative to the camera coordinate system origin are known. Thus, the azimuth and elevation of each intersection relative to the camera coordinate system origin can be simply computed. Let us say

21

that we have done this for a given intersection. Let us also say that
we have photographed the same intersection with the camera, and further,
that we have found the image coordinates of the intersection. These
coordinates can be used as input by the raytrace program, XLGEOM, to
calculate the azimuth and elevation. The azimuth and elevation calculated
in this way should agree exactly with those calculated from the survey
coordinates. If it does not, then the three nominal orientation angles
$(\theta, \epsilon, \delta)$ used by XLGEOM (stored in the calibration file) may be incorrect.
I have made the assumption that any discrepancy in azimuth between the
survey and raytrace derived object space coordinates for the intersection,
is entirely due to a camera azimuth bolt-down error. I have also made
the assumption that any discrepancy in elevation is due to an elevation
bolt-down error. This elevation offset is designated as ELOFFHI or
ELOFFLO in the calibration file, and is an additive correction to the
elevation (ELOFFHI is the additive elevation or bolt-down correction
which applies to high resolution imaging, and ELOFFLO applies to low
resolution imaging).

5.3   Calibration File Generation

5.3.1 Program GENGEOM

In Section 5.1, the format of the geometric calibration file was
defined. This file is generated by a simple interactive program, GENGEOM.
GENGEOM prompts the user for the various required values and gives him a
chance to review or dump out the numbers he has typed in prior to actually
writing them into the file. GENGEOM also has options to format a new
(empty) file or dump out (print) an existing file.

5.3.2   Program CMPRVL

CMPRVL performs the comparison of object space (azimuth and eleva-
tion) coordinates of grid target intersections derived in two ways: (1)
from a grid target survey, relative to the camera coordinate system origin,
and (2) from a raytrace, using the model described in Section 3.5.   CMPRVL
does this for all intersections and prints out the differences for each
intersection.   This allows one to see how close to reality ones camera
model, as contained in the calibration file, is.   If necessary, a new
file may be generated using GENGEOM, and CMPRVL may be run again to
check the accuracy of the new file.   This way, in very few iterations
(usually 3 or less), we can arrive at the optimum file (the one which
results in the minimum differences between survey and raytrace-derived
object space coordinates for the intersections.

5.4   Calibration File Data

Table 3 presents the calibration file data currently in use at IPL
by programs RANGER, GEOCAM and MARSCOR.   Lander number 3 refers to the
science test lander (STL), with the STC camera in position number 2 and
the FC-1A camera in position number 1.   Lander number 4 refers to the
STL with the STC camera in position number 2 and the STB camera in
position number 1.   Since the STB and FC-1A cameras have considerably
different azimuth bolt-down errors, such a distinction is necessary.

Table 3. Calibration File "Dump"

|	Lander 1 (FC-1)		Lander 2 (FC-2)		Lander 3 (STL)		Lander 4 (STL)	
	CAM 1	CAM 2	CAM 1	CAM 2	CAM 1	CAM 2	CAM 1	CAM 2
EPSILON	4.33845	0.73283	4.41176	2.57532	2.94978	-0.09547	2.97210	-0.09547
DELTA	0.00115	-0.00066	0.00050	-0.00074	0.0	0.0	0.0	0.0
THETA	1.34776	0.82587	1.41991	2.66747	0.0	0.0	0.0	0.0
PSACCR	0.0	-0.001	0.0	0.001	0.0	0.0	0.0	0.0
LENCOR	-0.024	-0.024	-0.021	-0.017	0.0	0.0	0.0	0.0
PSASFT	-0.0025	0.0	-0.001	-0.0065	0.0	0.0	0.0	0.0
PSAROT	-0.045	-0.697	0.5	0.003	0.0	0.0	0.0	0.0
ELOFF/HI	-0.00267	-0.00096	-0.0014	-0.00262	-0.000524	-0.001047	-0.000524	-0.001047
ELOFF/LOW	-0.00323	-0.00145	-0.0014	0.0	-0.000524	-0.001047	-0.000524	-0.001047
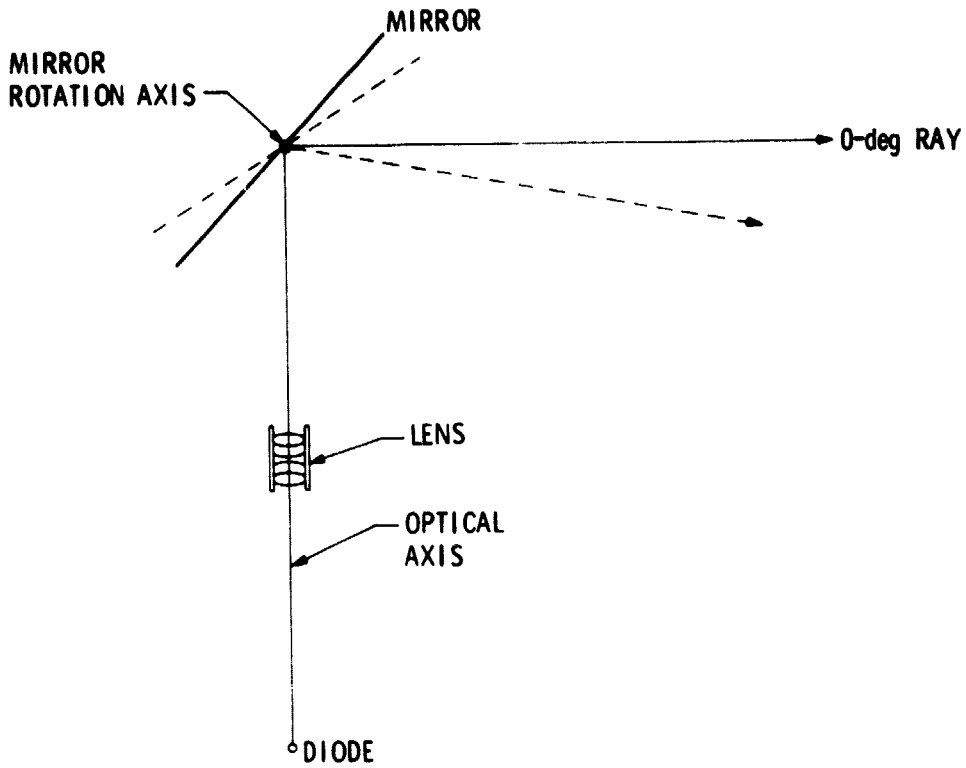
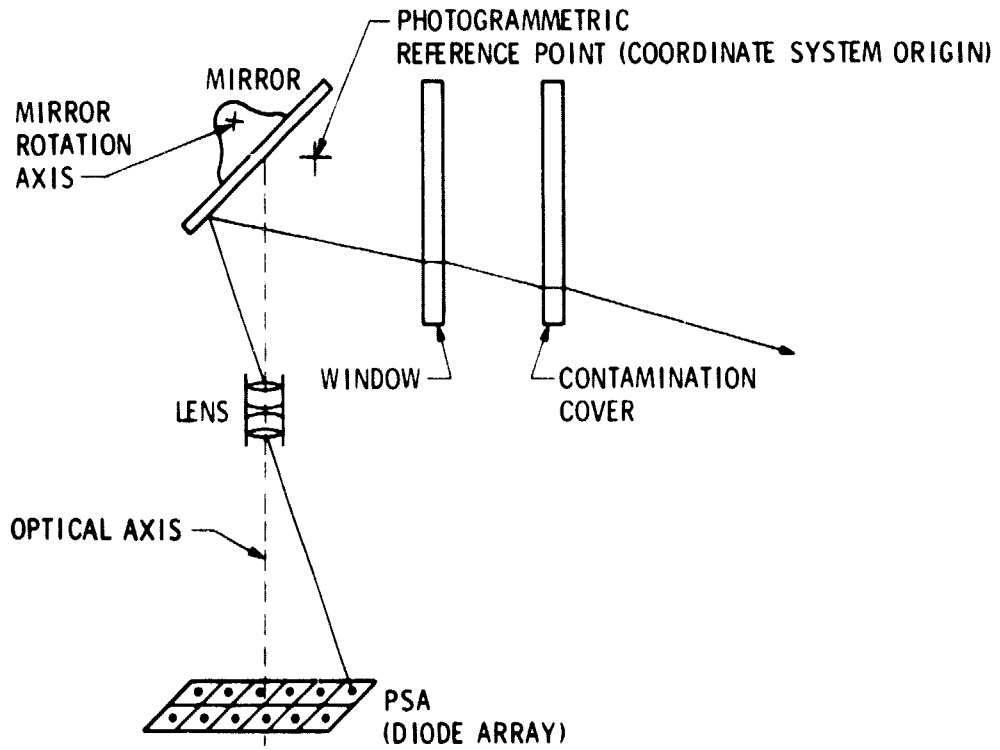Figure 1. Ideal Camera Optical System
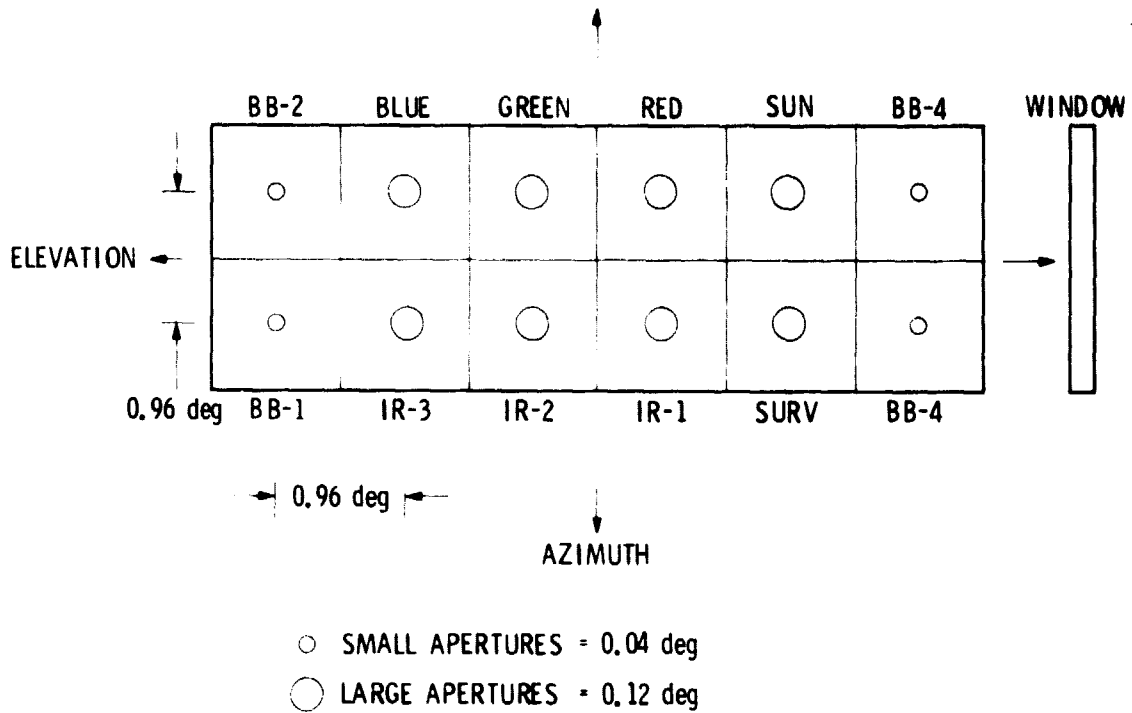

Figure 2. Actual Camera Optical System Geometry

BB-2   BLUE   GREEN   RED   SUN   BB-4   WINDOW

ELEVATION ←

0.96 deg   BB-1   IR-3   IR-2   IR-1   SURV   BB-4

←| 0.96 deg |→

AZIMUTH

○ SMALL APERTURES = 0.04 deg

◯ LARGE APERTURES = 0.12 deg

Figure 3.   PSA Alignment Diagram

AREA OF MINIZATION

-0.0174 deg AT 1.0 m

BB-3, -4   RED   GREEN   BB-1, -2

ELEVATION ANGLE, deg FOV

LOS DISPLACEMENT, in.
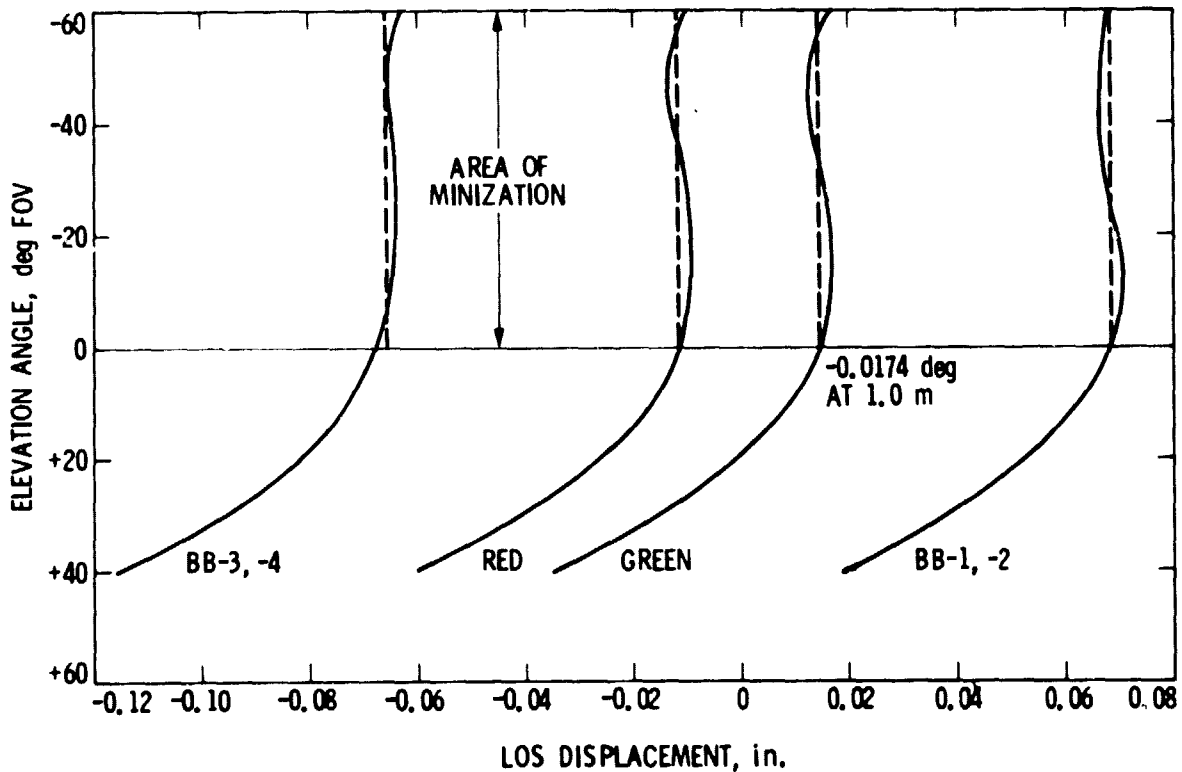
Figure 4.   Line-of-Sight Displacement Error
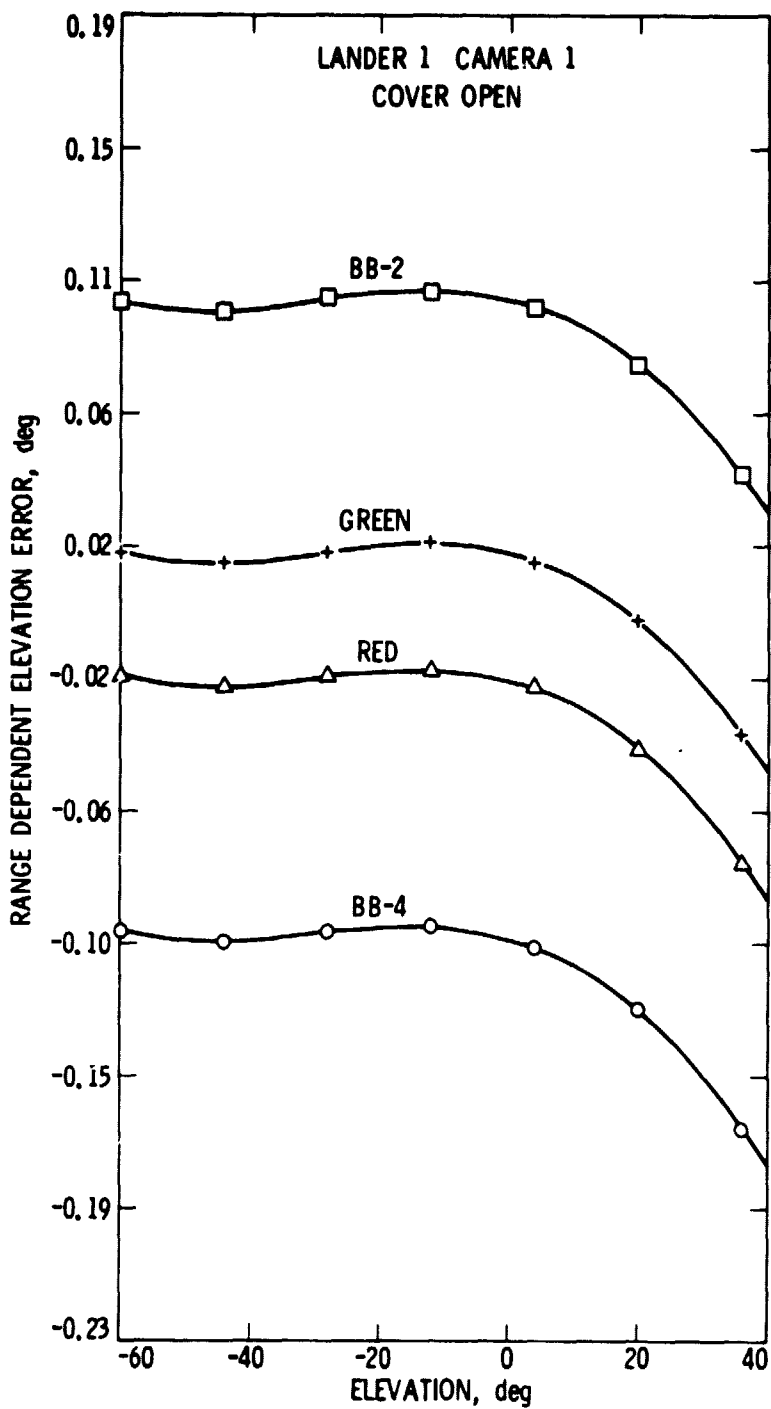
Figure 5. Range-Dependent Pointing Errors

MIRROR PLANE 1

MIRROR PLANE 2

MIRROR ROTATION AXIS

RAY FROM MIRROR PLANE 1

RAY
OFFSET

RAY FROM MIRROR PLANE 2

0.125 in.
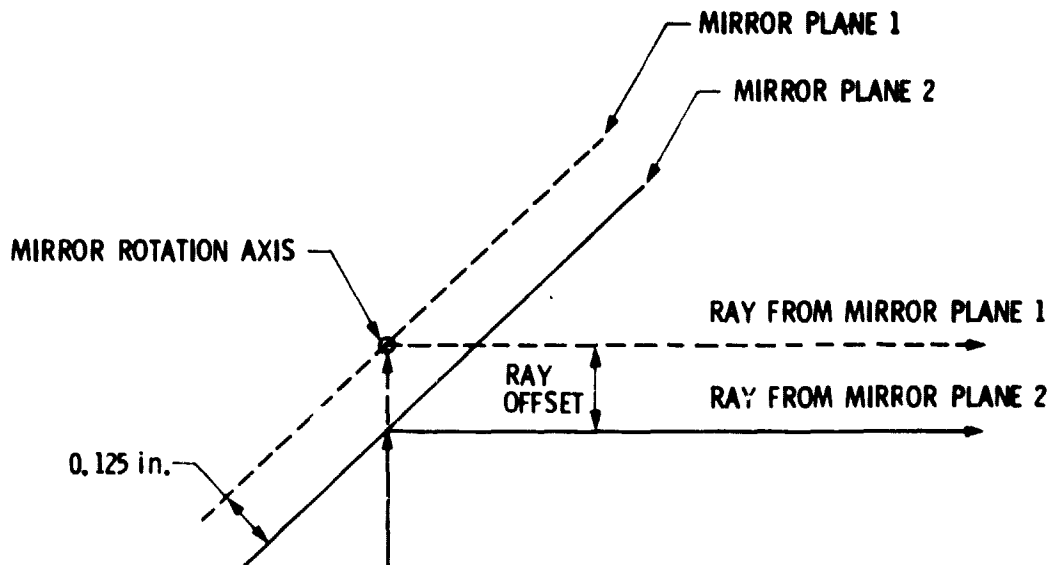
MIRROR PLANE 1: ROTATION AXIS LIES IN MIRROR PLANE
MIRROR PLANE 2: ROTATION AXIS LIES 32 cm. AWAY
FROM MIRROR PLANE
MIRROR ROTATION AXIS IS COMMON TO BOTH MIRROR
PLANES. ALSO, OFFSET INCREASES FOR RAY ELEVATIONS
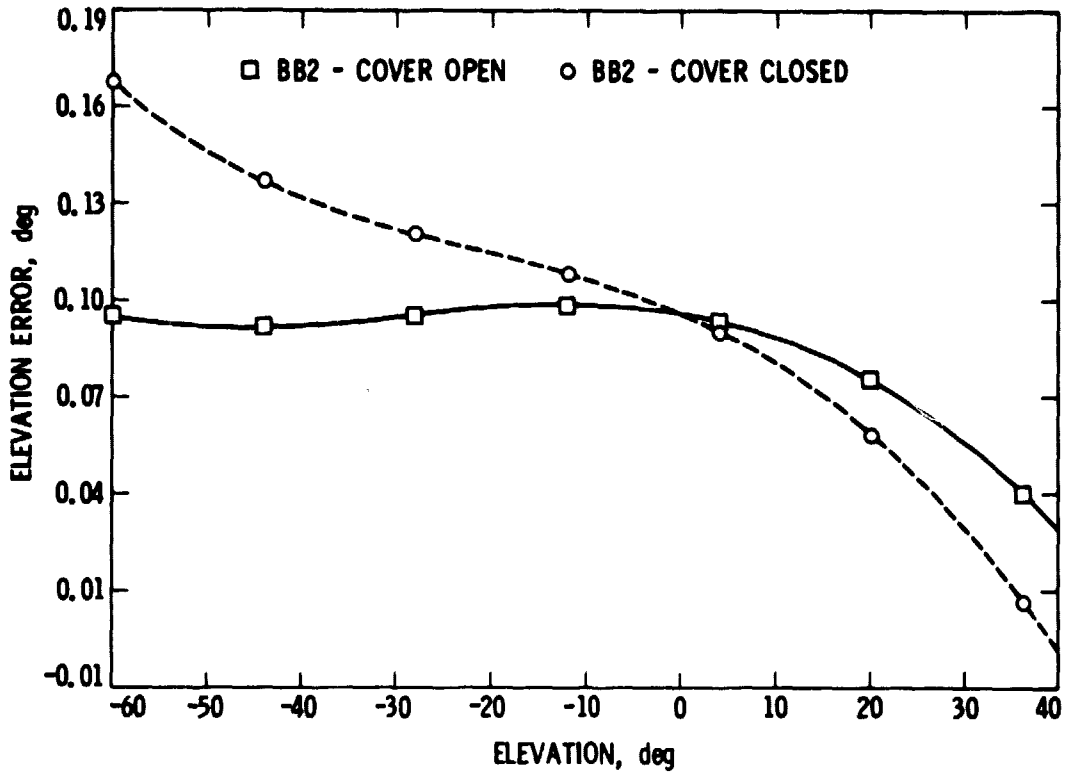BELOW 0 deg.

Figure 6. Mirror Planes

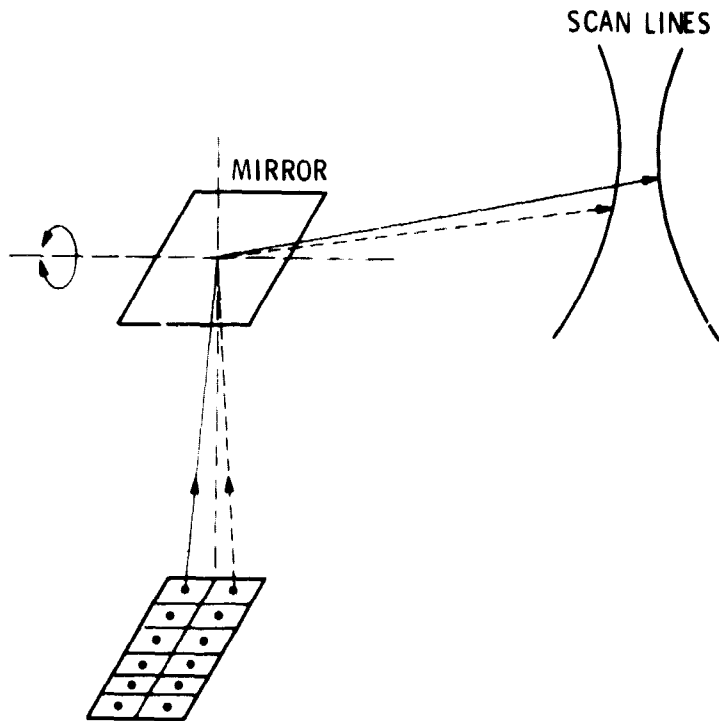Figure 7. Contamination Cover Effect on Range-Dependent Pointing Errors

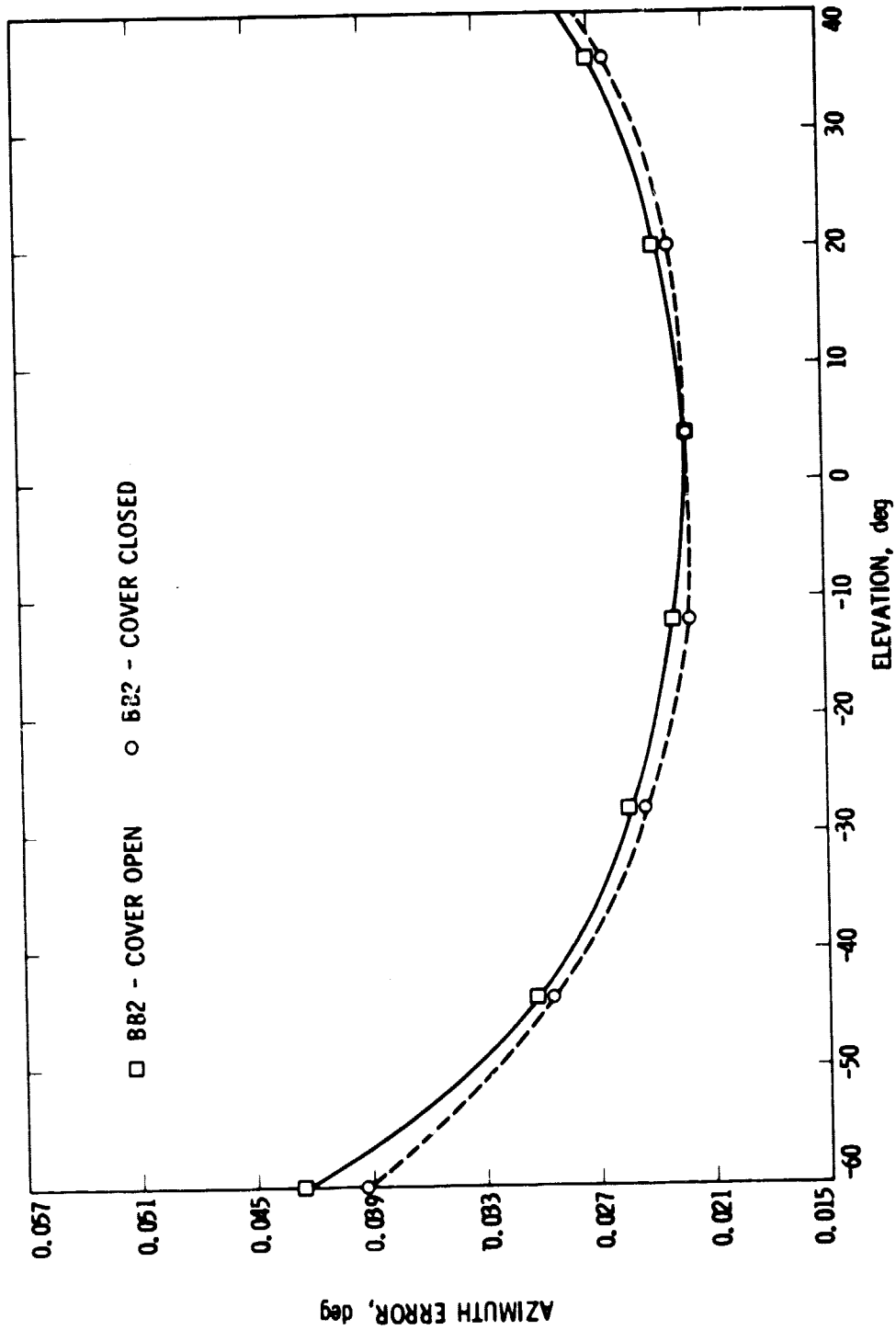Figure 8. "Coning Angle Correction" Diagram

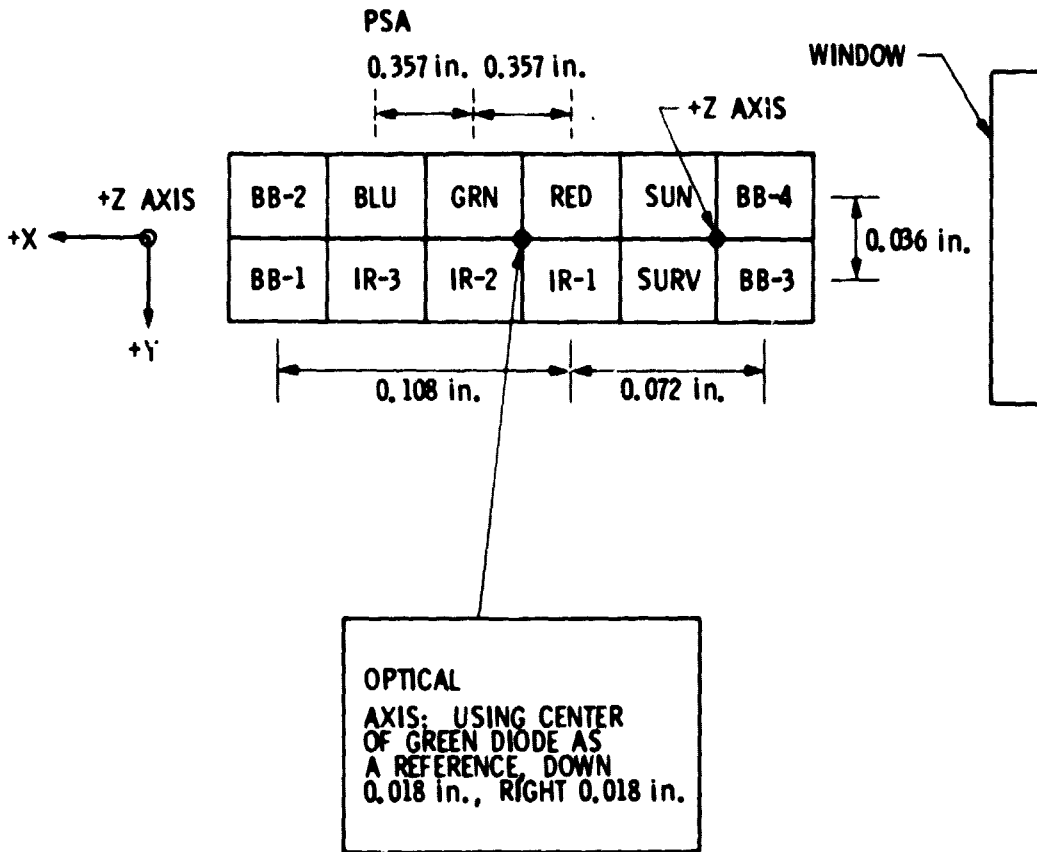Figure 9. Contamination Cover Effect on Diode Azimuth Offset Errors

30

Figure 10. Photosensor Array Layout - Lens Nodal Points
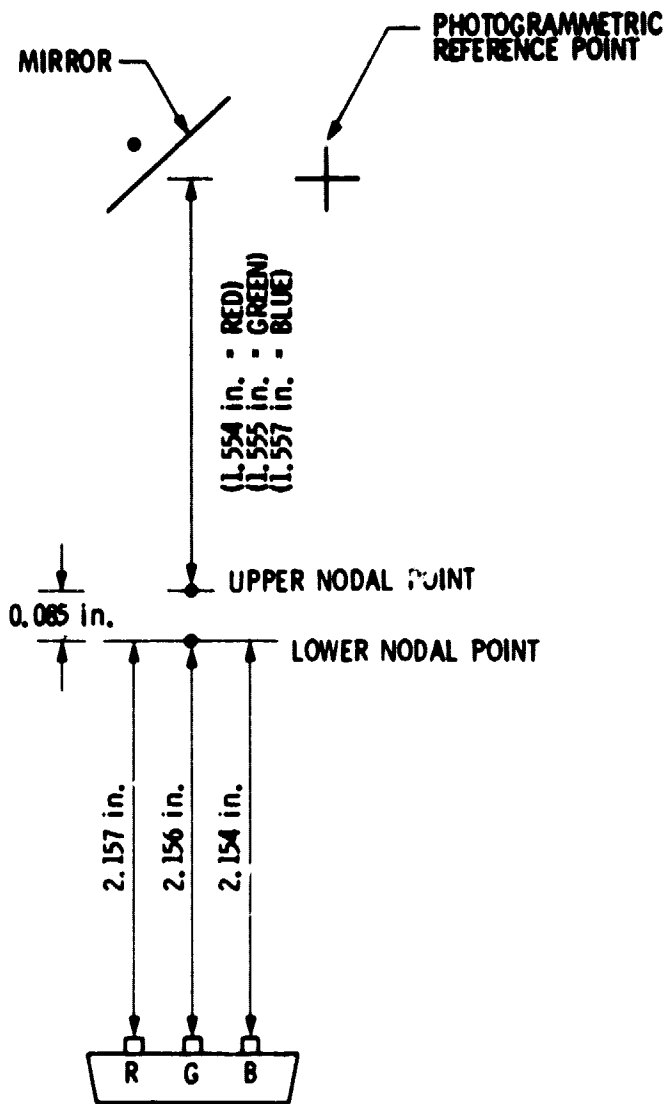
MIRROR

PHOTOGRAMMETRIC
REFERENCE POINT

(1.554 in. = RED)
(1.555 in. = GREEN)
(1.557 in. = BLUE)

UPPER NODAL POINT

0.085 in.

LOWER NODAL POINT

2.157 in.

2.156 in.

2.154 in.

R   G   B

PSA TO LOWER NODAL POINT   = 2.156 in.
LOWER TO UPPER NODAL POINT = 0.085 in.
UPPER NODAL POINT TO ZERO
ELEVATION PLANE   = 1.555 in.

Figure 11. Lens Nodal Points
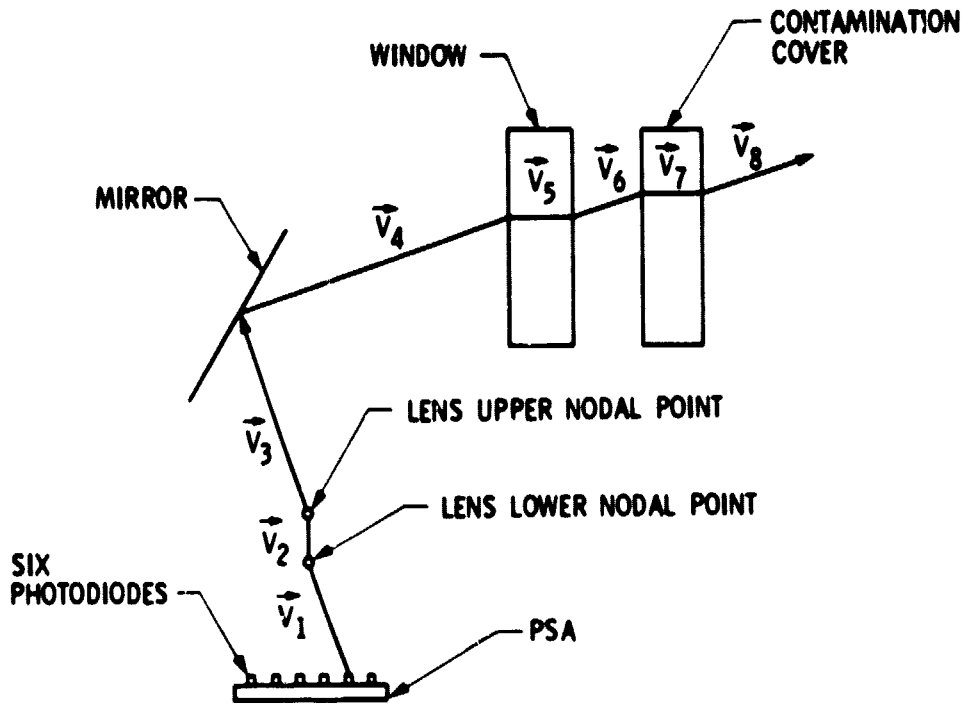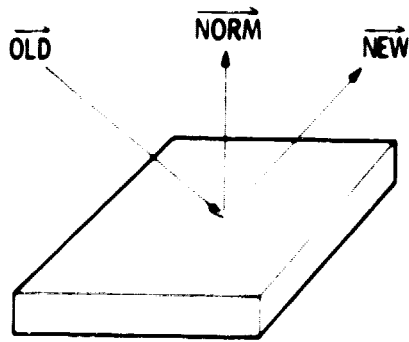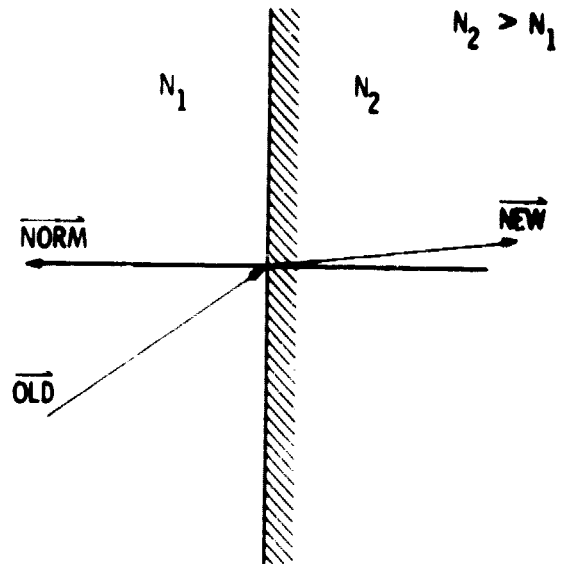
WINDOW

CONTAMINATION COVER

$\vec{V_5}$ $\vec{V_6}$ $\vec{V_7}$ $\vec{V_8}$

MIRROR

$\vec{V_4}$

LENS UPPER NODAL POINT

$\vec{V_3}$

LENS LOWER NODAL POINT

$\vec{V_2}$

SIX PHOTODIODES

$\vec{V_1}$

PSA

Figure 12. Raytrace Vector Diagram

$\overrightarrow{OLD}$ $\overrightarrow{NORM}$ $\overrightarrow{NEW}$

$N_2 > N_1$

N_1 $\qquad$ N_2

$\overrightarrow{NORM}$

$\overrightarrow{NEW}$

$\overrightarrow{OLD}$

$$\overrightarrow{OLD} \cdot \overrightarrow{NORM} = -\overrightarrow{NEW} \cdot \overrightarrow{NORM}$$

$$\overrightarrow{NEW} \cdot (\overrightarrow{OLD} \times \overrightarrow{NORM}) = 0$$

$$\left[(\overrightarrow{OLD} \cdot \overrightarrow{NORM}) \overrightarrow{NORM} - \overrightarrow{OLD}\right] \cdot \overrightarrow{OLD} =$$
$$\left[(\overrightarrow{OLD} \cdot \overrightarrow{NORM}) \overrightarrow{NORM} - \overrightarrow{OLD}\right] \cdot \overrightarrow{NEW}$$

$$N_1^2 - N_1^2 (\overrightarrow{OLD} \cdot \overrightarrow{NORM})^2 = N_2^2 - N_2^2 (\overrightarrow{NEW} \cdot \overrightarrow{NORM})^2$$

$$N_1 \left[(\overrightarrow{OLD} \cdot \overrightarrow{NORM}) \overrightarrow{NORM} - \overrightarrow{OLD}\right] \cdot \overrightarrow{OLD} =$$
$$N_2 \left[(\overrightarrow{OLD} \cdot \overrightarrow{NORM}) \overrightarrow{NORM} - \overrightarrow{OLD}\right] \cdot \overrightarrow{NEW}$$

$$\overrightarrow{NEW} \cdot (\overrightarrow{OLD} \times NORM) = 0$$

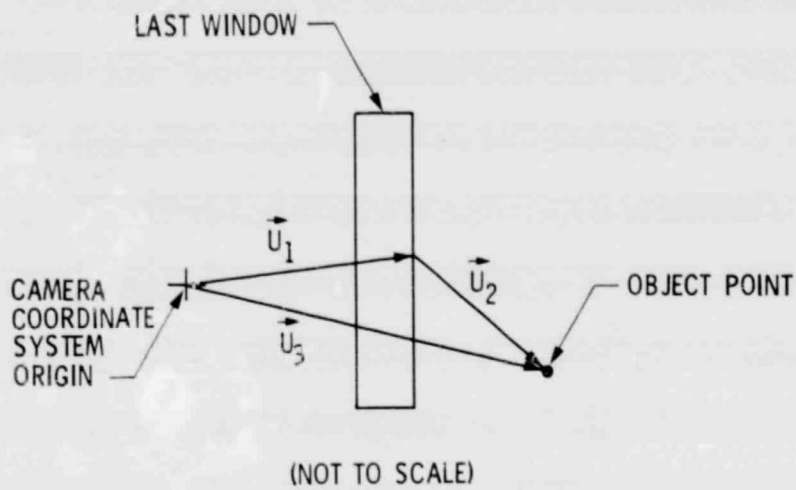Figure 13. Vector Diagrams and Equations for Raytrace

33

(NOT TO SCALE)

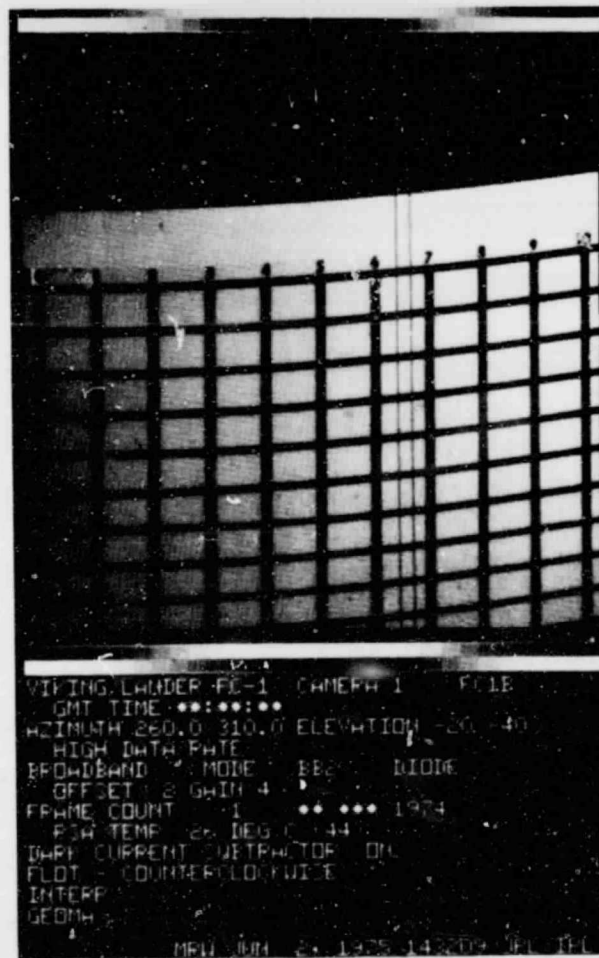Figure 14. Range Vector Diagram

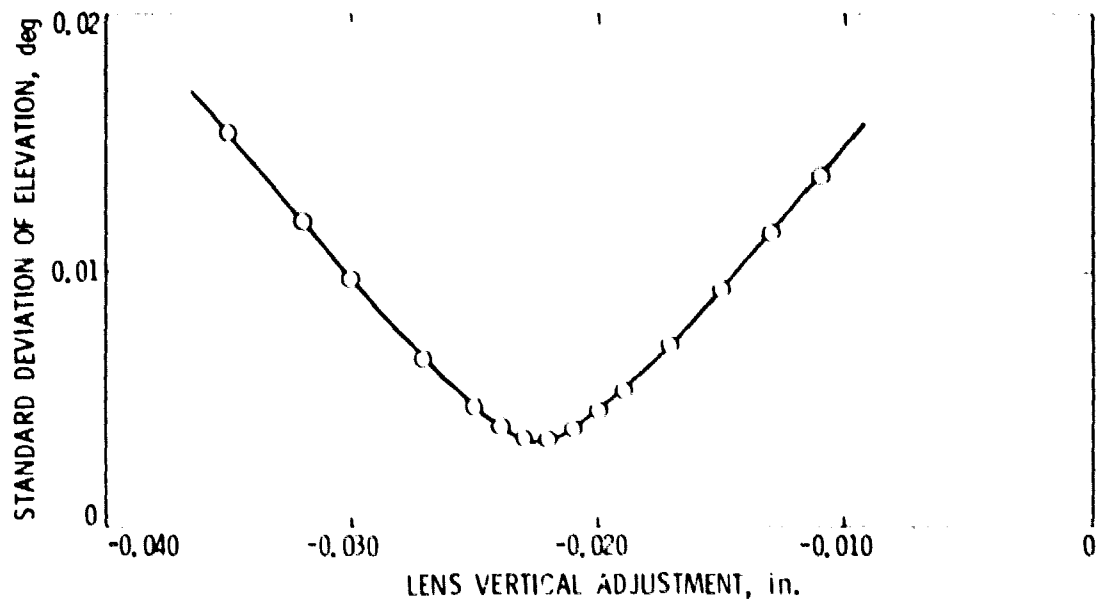Figure 15. Grid Target Image, Lander 1, Camera 1, MMA

34

Figure 16. Convergence Curve From Program "VLOPTICS"

```
 VLOPTICS HERE
 FOR PRINTOUT TYPE YES
↑YES"
 FOR DEFAULT COORDS TYPE YES
↑YES"
 INPUT LENCOR DELTA,LOW AND HIGH LIMITS:
↑.01,-.04,.04"
 INPUT PSHCOR DELTA, LOW AND HIGH LIMITS
↑.01,-.04,.05"
 INPUT ICONT, ELCOM, RANGE:
↑0,-20.,2."
 INPUT PSHROT DELTA, LOW AND HIGH LIMITS
↑.01,-.04,.04"
 INPUT INITIAL PSAROT VALUE
↑-.04"
 INPUT PSASFT DELTA, HIGH AND LOW LIMITS
↑.01,-.04,.04"
 SD= 0.0206812   LENCOR=-0.0400   ST= 0.0333536
 SD= 0.0168157   LENCOR=-0.0300   ST= 0.0363497
 SD= 0.0060010   LENCOR=-0.0200   ST= 0.0388246
 SD= 0.0086160   LENCOR=-0.0100   ST= 0.0412821
 SD= 0.0197355   LENCOR= 0.0000   ST= 0.0437181
 SD= 0.0312110   LENCOR= 0.0100   ST= 0.0461348
 SD= 0.0426674   LENCOR= 0.0200   ST= 0.0485361
 SD= 0.0540687   LENCOR= 0.0300   ST= 0.0509204
 SD= 0.0414705   PSHCOR=-0.0400   ST= 0.0482868
 SD= 0.0303126   PSHCOR=-0.0300   ST= 0.0459498
 SD= 0.0191424   PSHCOR=-0.0200   ST= 0.0435895
 SD= 0.0083606   PSHCOR=-0.0100   ST= 0.0412185
 SD= 0.0060010   PSHCOR= 0.0000   ST= 0.0388246
 SD= 0.0165202   PSHCOR= 0.0100   ST= 0.0364130
 SD= 0.0280700   PSHCOR= 0.0200   ST= 0.0339849
 SD= 0.0398796   PSHCOR= 0.0300   ST= 0.0315421
 SD= 0.0518182   PSHCOR= 0.0400   ST= 0.0290806
LENCOR=-0.0200   PSHCOR= 0.0000   SD= 0.0060010
 SD= 0.0388277   PSHROT=-0.0350 DEGREES
***↑"SD= 0.0388366   PSHROT=-0.0250 DEGREES
 SD= 0.0388416   PSHROT=-0.0150 DEGREES
 SD= 0.0388727   PSHROT=-0.0050 DEGREES
 SD= 0.0388943   PSHROT= 0.0050 DEGREES
 SD= 0.0389259   PSHROT= 0.0150 DEGREES
 SD= 0.0389621   PSHROT= 0.0250 DEGREES
 SD= 0.0390024   PSHROT= 0.0350 DEGREES
 SD= 0.4460843   PSHSFT=-0.0400
 SD= 0.4450016   PSHSFT=-0.0300
 SD= 0.4438959   PSASFT=-0.0200
 SD= 0.0377444   PSHSFT=-0.0100
 SD= 0.0388277   PSHSFT= 0.0000
 SD= 0.0400617   PSHSFT= 0.0100
 SD= 0.4393618   PSHSFT= 0.0200
 SD= 0.4381931   PSASFT= 0.0300



 BEST VALUES ARE....


 LENCOR= -0.0200
 PSACOR=  0.0000
 PSAROT= -0.0350
 PSASFT= -0.0100
```

Figure 17. Printout From Program "VLOPTICS"